Supplementary Information

Spin-Polarized Electron Transfer in Chiral Tartaric Acid-Engineered $Ni(OH)_2$ Unlocks NiOOH Activation for Urea Electrooxidation

Ming Chen,[a] Wen-Da Zhang,[a,]* Qingna Gong,[a] Jiangyong Liu,[b] Xiaoping Yang,[c] Jing Wang[a,]* and Xiaodong Yan[a,c]*

[a] Key Laboratory of Synthetic and Biological Colloids, Ministry of Education, School of Chemical and Material Engineering, Jiangnan University, Wuxi 214122, P.R. China
E-mail address: wenda.zhang94@gmail.com; jingwang@jiangnan.edu.cn; xiaodong.yan@jiangnan.edu.cn
[b] School of Chemistry and Chemical Engineering, Yangzhou University, Yangzhou 225002, P.R. China
[c] State Key Laboratory of Organic-Inorganic Composites, Beijing University of Chemical Technology, Beijing 10029, P.R. China

1. Experimental section

1.1 Reagents

Nickel nitrate hexahydrate ($Ni(NO_3)_2·6H_2O$), cobalt nitrate hexahydrate ($Co(NO_3)_2·6H_2O$), hydrochloric acid (HCl), and ethanol (C_2H_5OH) were purchased from Sinopharm Group. Potassium hydroxide (KOH), urea ($CO(NH_2)_2$), D-tartaric acid (D-TA), L-tartaric acid (L-TA), DL-tartaric acid (DL-TA), D-malic acid (D-MA), L-malic acid (L-MA), and DL-malic acid (DL-MA) were obtained from Energy Chemical. Nickel foam (NF) was supplied by Suzhou Sinero Technology Co., LTD. All water used is deionized (DI).

1.2 Synthesis of $Ni(OH)_2$ catalyst

NF (3 × 3 cm^2) was sequentially ultrasonicated in 3 M HCl, deionized water, and absolute ethanol for 10 min each. The cleaned NF was then dried at 60°C for 12 h. A total of 2 mmol $Ni(NO_3)_2·6H_2O$ (581.58 mg) was dissolved in 29 mL of deionized water and transferred into a 50 mL Teflon-lined autoclave. After thorough stirring, 1 mL of 1 M NaOH solution was added and mixed until homogeneous. The cleaned NF was then immersed in the solution, and the autoclave was sealed in a stainless steel reactor. The reaction was conducted at 120°C for 10 h. After cooling to room temperature, the NF was removed and dried to obtain $Ni(OH)_2$/NF.

1.3. Synthesis of chiral molecule modified $Ni(OH)_2$ catalysts

Based on step 1.2, 1 mmol D-TA, L-TA, or DL-TA (150.09 mg) was added, and the reaction procedure was repeated under identical conditions. The same protocol was applied for D-MA, L-MA, DL-MA, and $Co(NO_3)_2·6H_2O$ using equivalent amounts. The TA-modified $Ni(OH)_2$ samples were named D-TA- $Ni(OH)_2$/NF, L-TA-Ni $Ni(OH)_2$/NF, and DL-TA- $Ni(OH)_2$/NF, respectively. Similarly, the MA-modified $Ni(OH)_2$ samples were designated as D-MA- $Ni(OH)_2$/NF, L-MA- $Ni(OH)_2$/NF, and DL-MA- $Ni(OH)_2$/NF, while the TA-modified $Co(OH)_2$ samples were labeled as D-TA-$Co(OH)_2$/NF, L-TA-$Co(OH)_2$/NF, and DL-TA-$Co(OH)_2$/NF, respectively.

2. Characterizations

X-ray diffraction (XRD) spectrum was measured via utilizing Shimadzu XRD 6000 X ray diffractometer. An evaluation of morphology was conducted utilizing the scanning electron microscope (SEM) Zeiss Ultra SEM and the transmission electron microscope (TEM) JEOL JEM 2100. Energy dispersive X-ray spectroscopy (EDS) measurement was equipped. XPS spectrum was obtained using a Thermo Fisher ESCALAB 250Xi. The XPS spectrum was adjusted using C 1s line at 284.8 eV as a criterion. Raman spectroscopy analysis was conducted using a Renishaw inVia reflex Raman spectrometer.

3. Electrochemical tests

All electrochemical assessment data were assessed at atmospheric temperature with the three-electrode system using a CHI760E electrochemical workstation. The reference counter, and working electrodes are an Hg/HgO electrode, a platinum plate, and NF loaded with catalysts (1 × 1 cm^2), respectively. A solution of 1.0 M KOH + 0.33 M urea was utilized to be the electrolyte during the urea oxidation reaction (UOR) performance tests, and 1.0 M KOH without 0.33 M urea was used during the oxygen evolution reaction (OER) performance tests. The linear sweep voltammetry (LSV) tests were conducted under a sweep rate of 5 mV s^{-1}. All LSV curves obtained were IR corrected. Cyclic voltammetry (CV) curves were documented under a sweeping rate from 20 - 100 mV s^{-1} within a potential ranging from 0 - 0.1 V vs. Hg/HgO to evaluate the double-layer capacitance (C_{dl}) of the catalysts. The data of Electrochemical impedance spectroscopy (EIS) measurements was obtained at 0.5 V vs. Hg/HgO. Additionally, the stability of the catalysts was evaluated by chronoamperometry without iR correction. All potentials were recalibrated to reversible hydrogen electrode (RHE) scale using the equation:

$$E_{RHE} = E_{Hg/HgO} + 0.059 * pH + 0.098$$

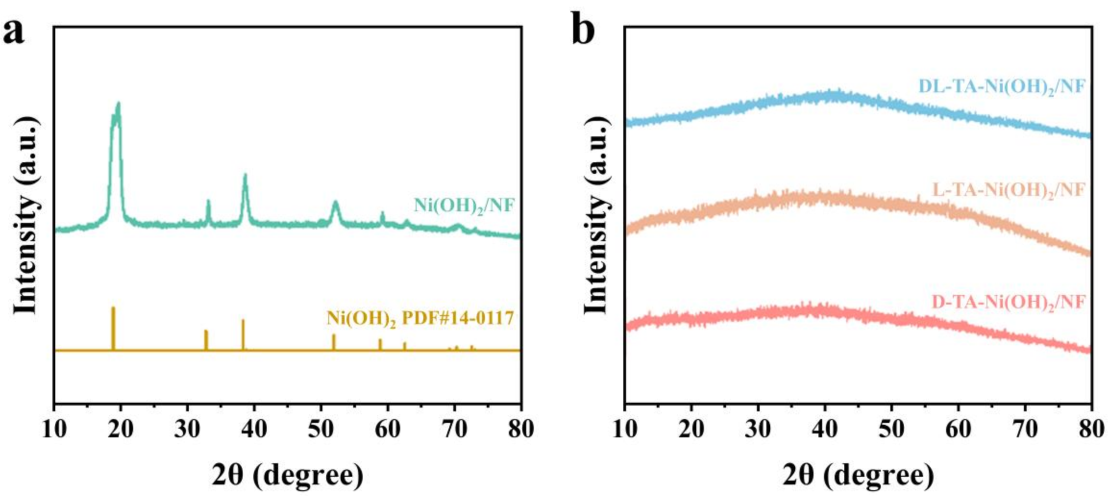

Fig. S1 XRD profiles of (a) Ni(OH)$_2$/NF and (b) DL-TA-Ni(OH)$_2$/NF, L-TA-Ni(OH)$_2$/NF and D-TA-Ni(OH)$_2$/NF.

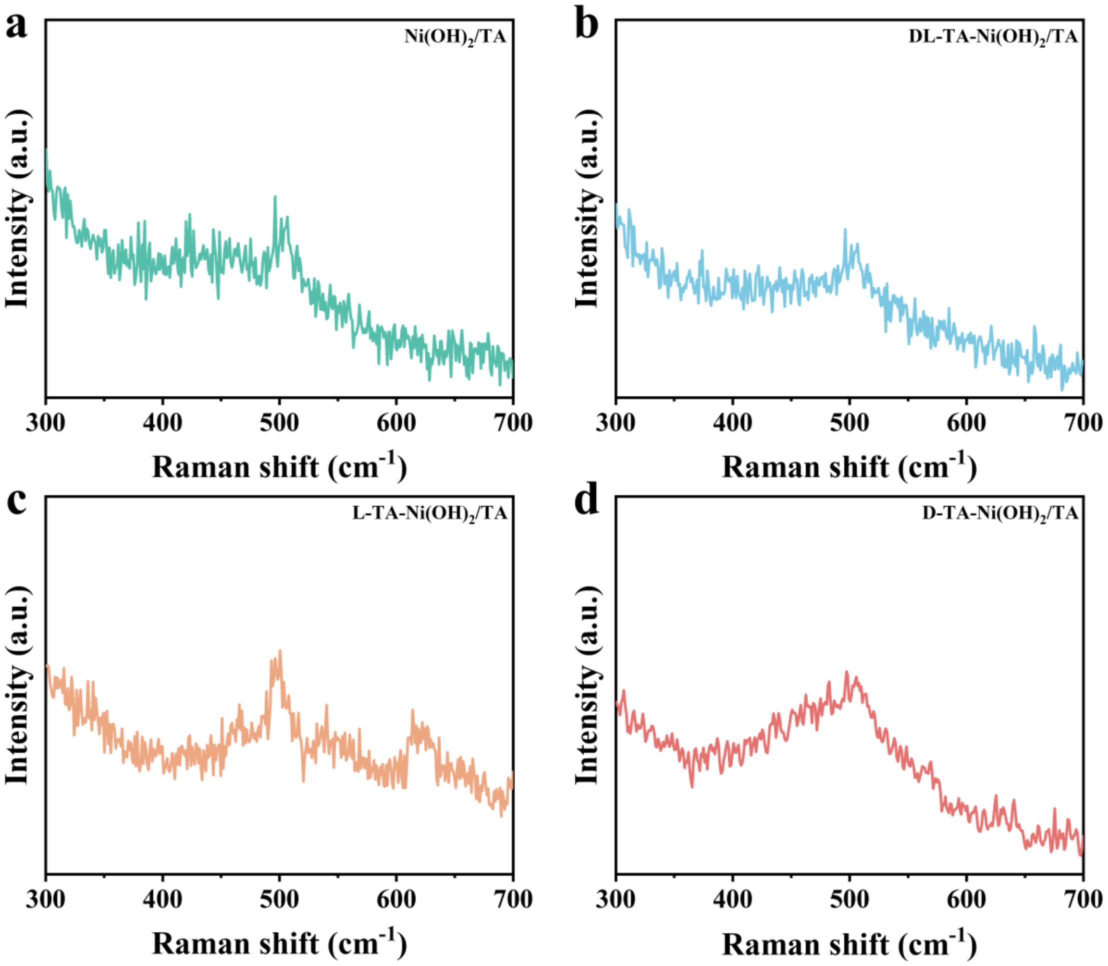

Fig. S2 Raman spectra of (a) $Ni(OH)_2$/NF, (b) DL-TA-$Ni(OH)_2$/NF, (c) L-TA-$Ni(OH)_2$/NF and (d) D-TA-$Ni(OH)_2$/NF at 1.30 V.

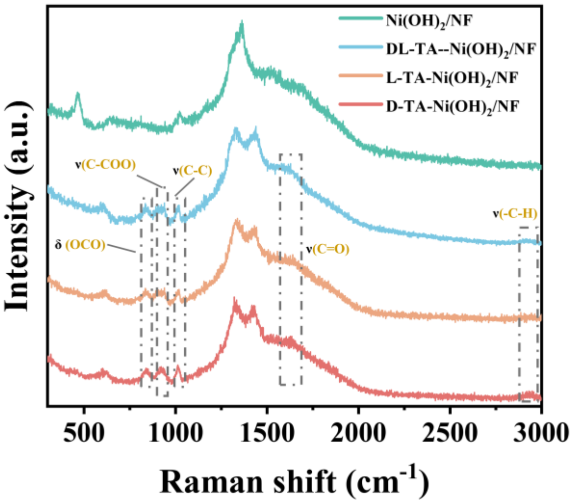

Fig. S3 Raman spectra of $Ni(OH)_2$/NF, DL-TA-$Ni(OH)_2$/NF, L-TA-$Ni(OH)_2$/NF and D-TA-$Ni(OH)_2$/NF.

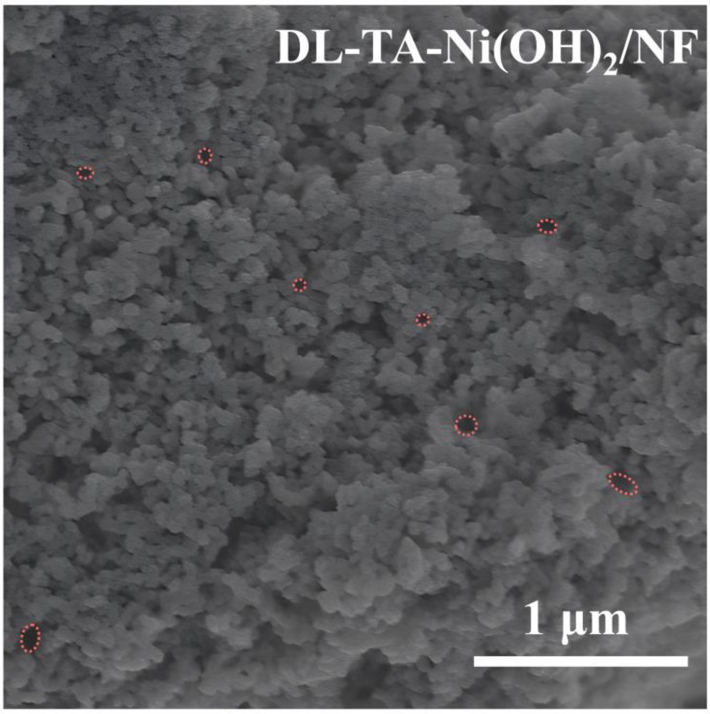

Fig. S4 SEM image of DL-TA-Ni(OH)$_2$/NF.

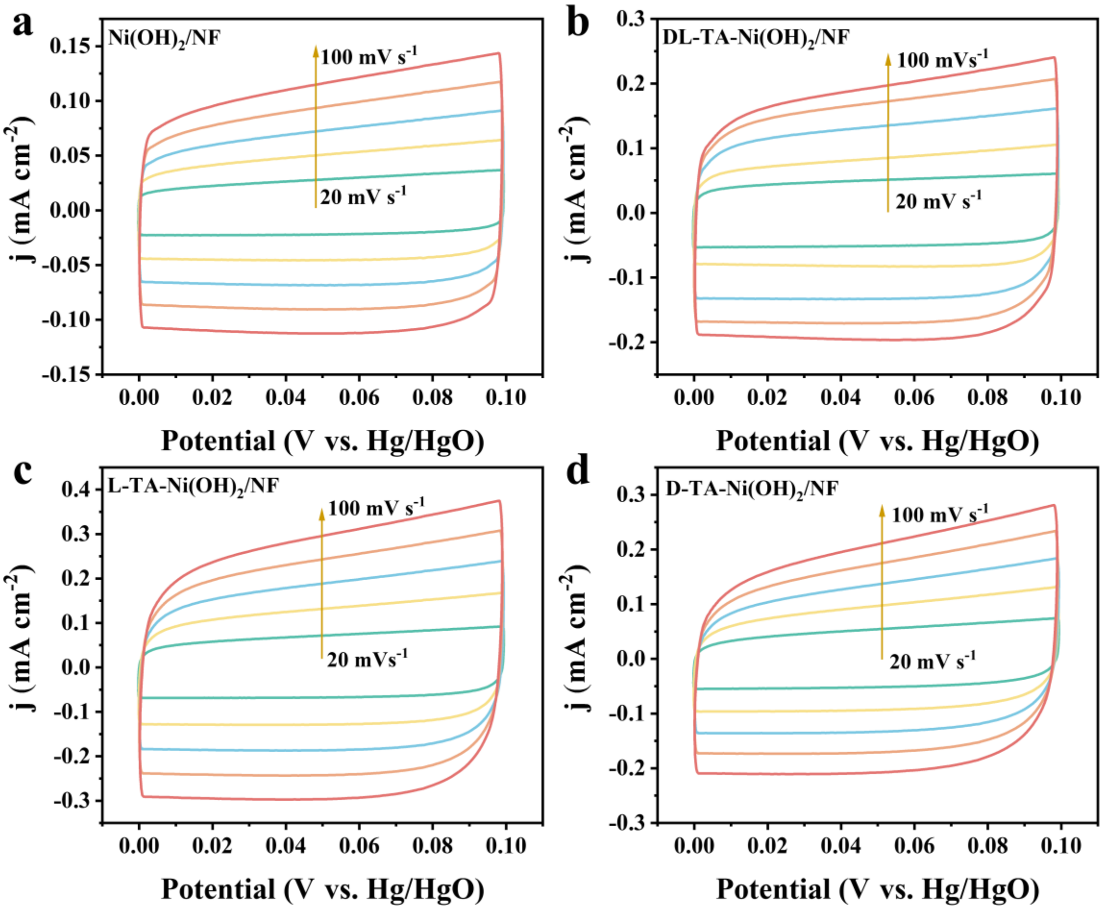

Fig. S5 CV curves of (a) $Ni(OH)_2$/NF, (b) DL-TA- $Ni(OH)_2$/NF, (c) L-TA- $Ni(OH)_2$/NF and (d) D-TA-$Ni(OH)_2$/NF

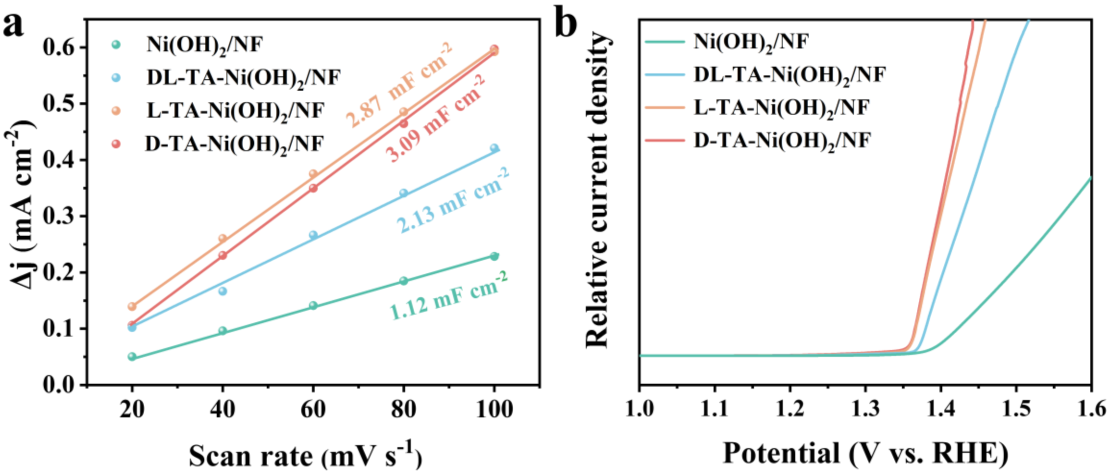

Fig. S6 (a) C_{dl} values and (b) ECSA-normalized LSV curves of $Ni(OH)_2$/NF, DL-TA-$Ni(OH)_2$/NF, L-TA- $Ni(OH)_2$/NF and D-TA-$Ni(OH)_2$/NF.

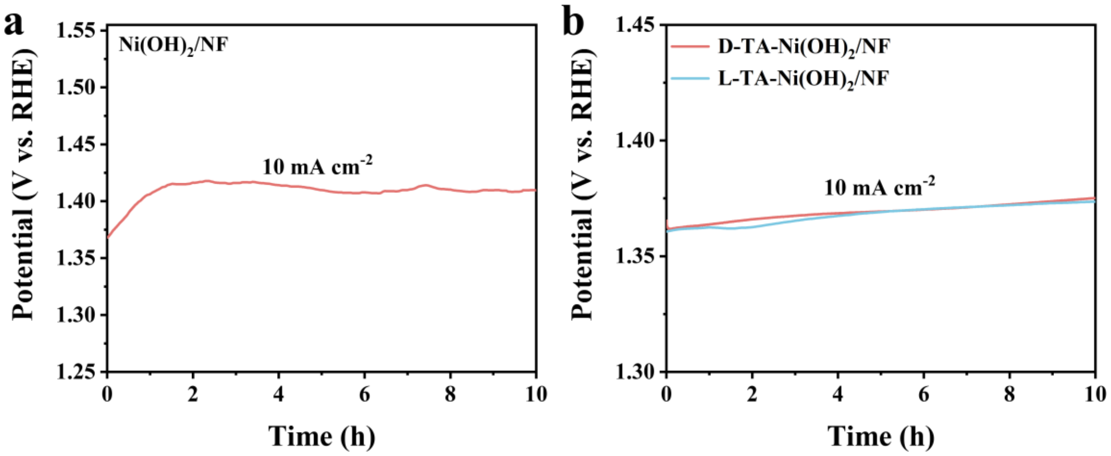

Fig. S7 Stability tests of (a) $Ni(OH)_2$/NF and (b) L-TA-$Ni(OH)_2$/NF and D-TA-$Ni(OH)_2$/NF at 10 mA cm^{-2}.

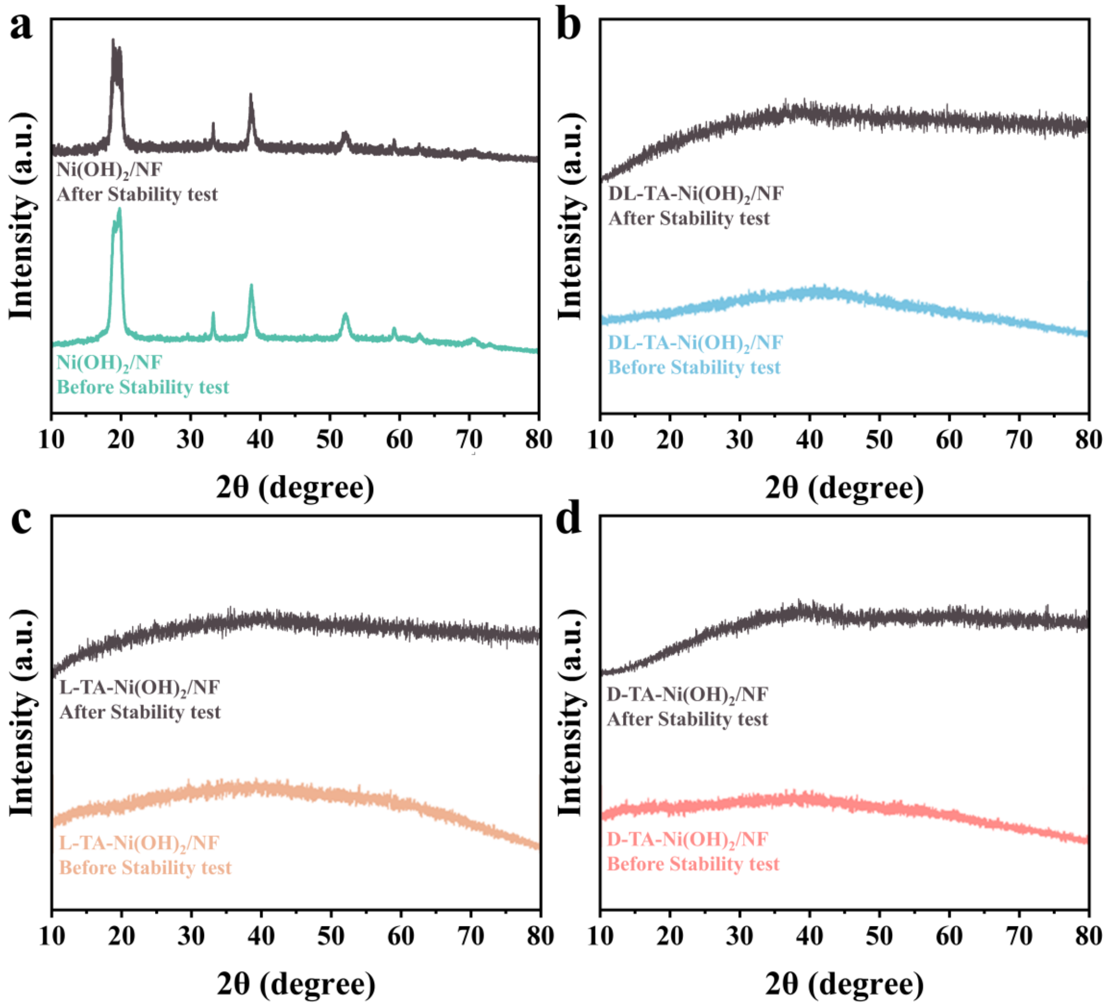

Fig. S8 XRD profiles of (a) $Ni(OH)_2$/NF and (b) DL-TA-$Ni(OH)_2$/NF, L-TA-$Ni(OH)_2$/NF and D-TA-$Ni(OH)_2$/NF after stability tests.

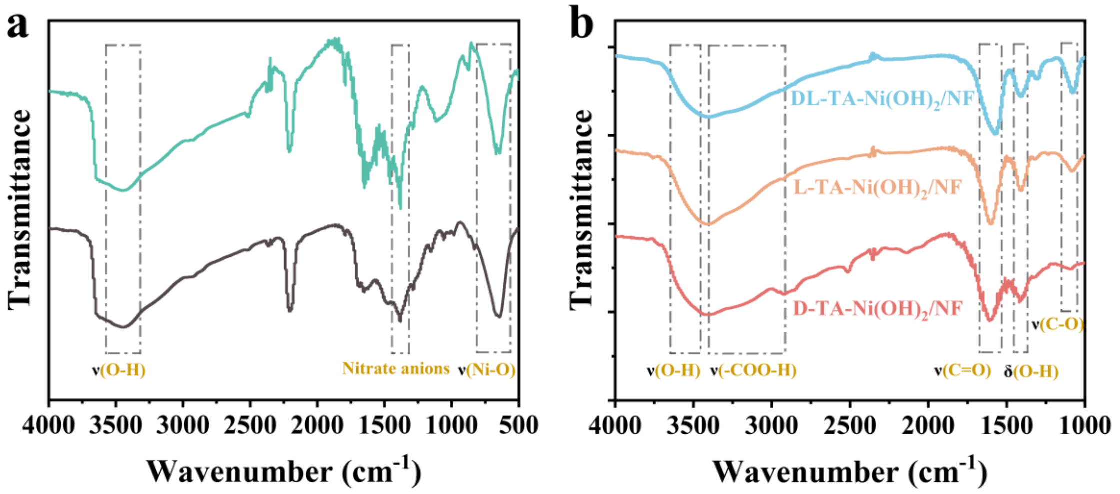

Fig. S9 (a) FT-IR spectra of $Ni(OH)_2$/NF before (Green line) and after (Grey line) stability test. (b) FT-IR spectra of DL-TA-$Ni(OH)_2$/NF, L-TA-$Ni(OH)_2$/NF and D-TA-$Ni(OH)_2$/NF after stability tests.

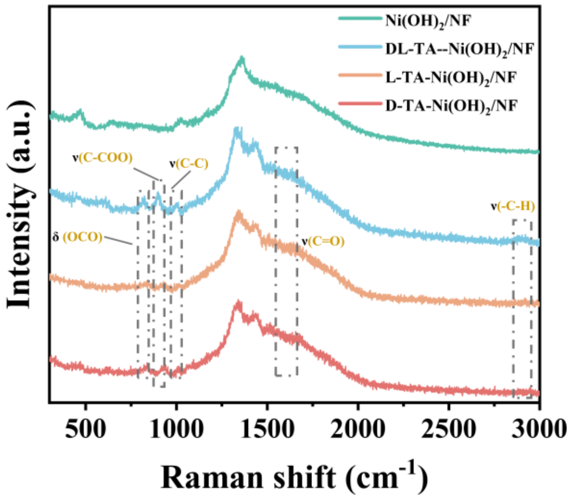

Fig. S10 Raman spectra of $Ni(OH)_2$/NF, DL-TA-$Ni(OH)_2$/NF, L-TA-$Ni(OH)_2$/NF and D-TA-$Ni(OH)_2$/NF after stability tests.

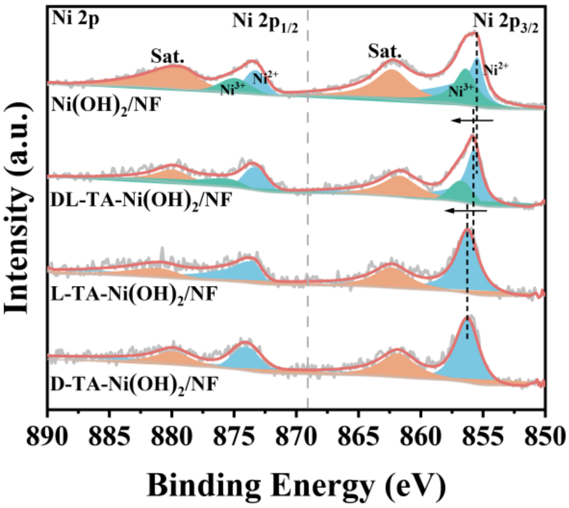

Fig. S11 Ni 2p spectra of $Ni(OH)_2$/NF, DL-TA-$Ni(OH)_2$/NF, L-TA-$Ni(OH)_2$/NF and D-TA-$Ni(OH)_2$/NF after stability tests.

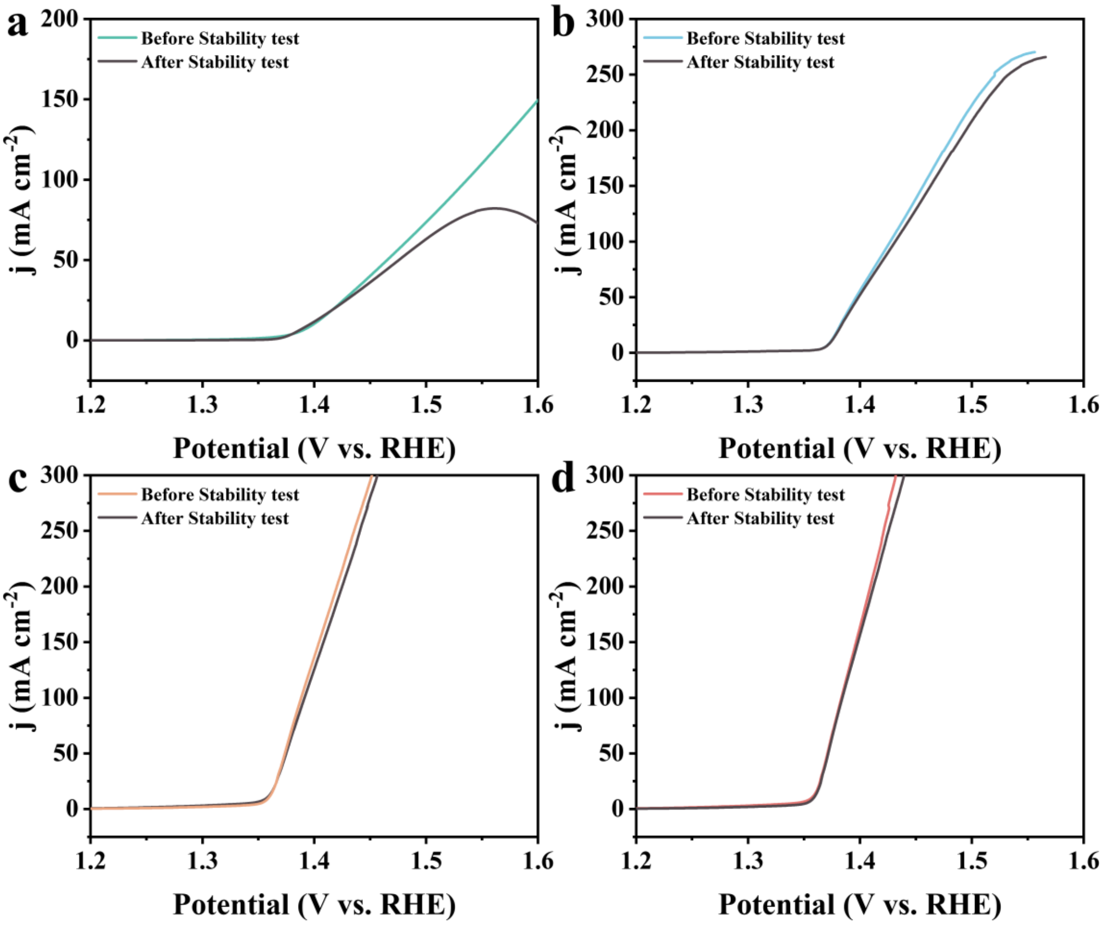

Fig. S12 LSV curves of (a) $Ni(OH)_2$/NF, (b) DL-TA- $Ni(OH)_2$/NF, (c) L-TA- $Ni(OH)_2$/NF and (d) D-TA-$Ni(OH)_2$/NF after stability tests.

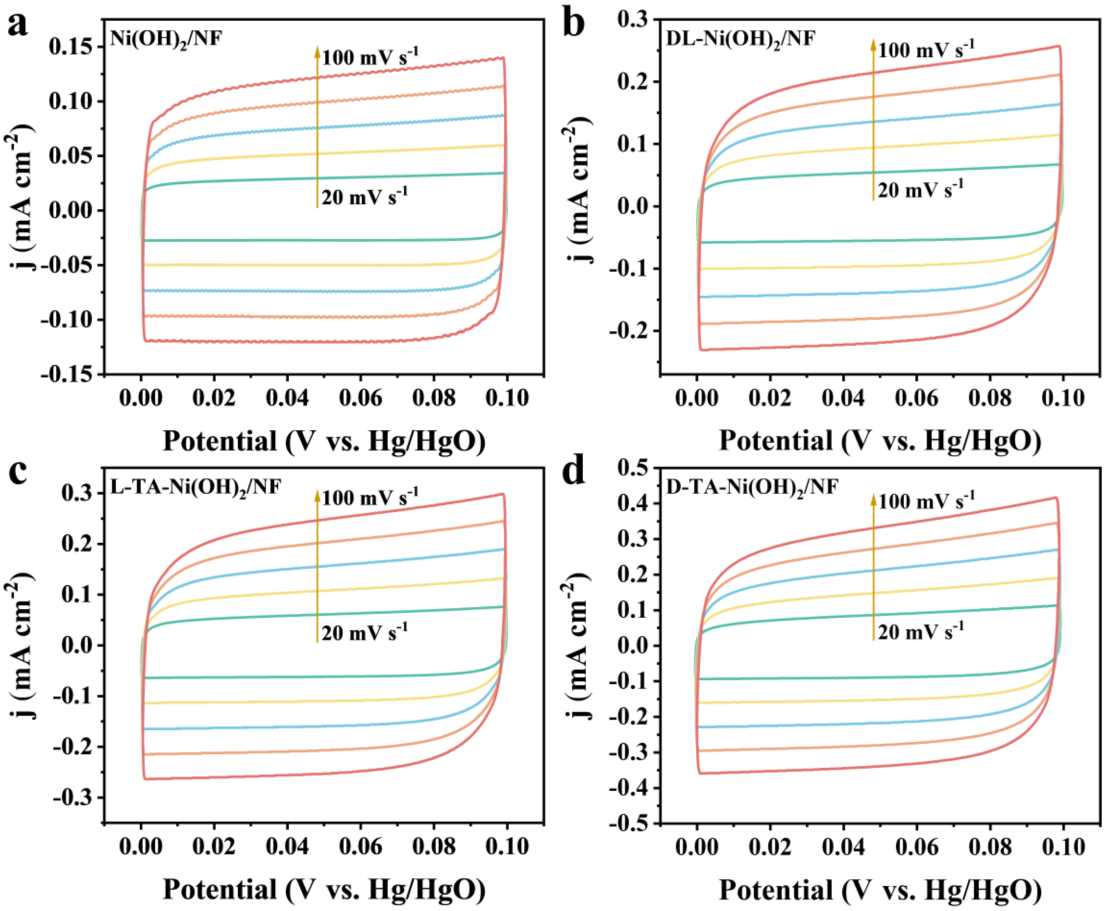

Fig. S13 CV curves of (a) $Ni(OH)_2$/NF, (b) DL-TA- $Ni(OH)_2$/NF, (c) L-TA- $Ni(OH)_2$/NF and (d) D-TA-$Ni(OH)_2$/NF after stability tests.

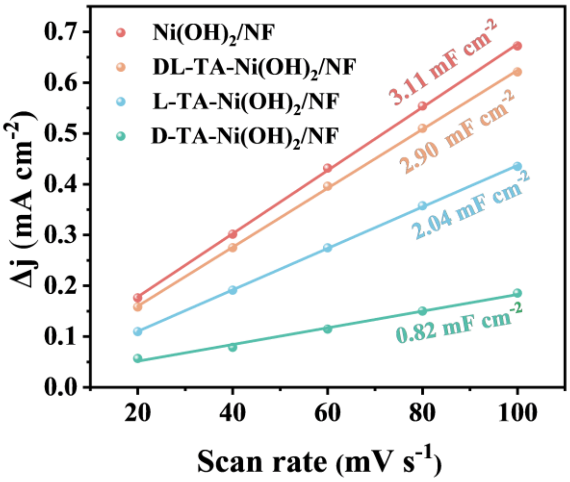

Fig. S14 C_{dl} values of $Ni(OH)_2$/NF, DL-TA- $Ni(OH)_2$/NF, L-TA- $Ni(OH)_2$/NF and D-TA-$Ni(OH)_2$/NF after stability tests.

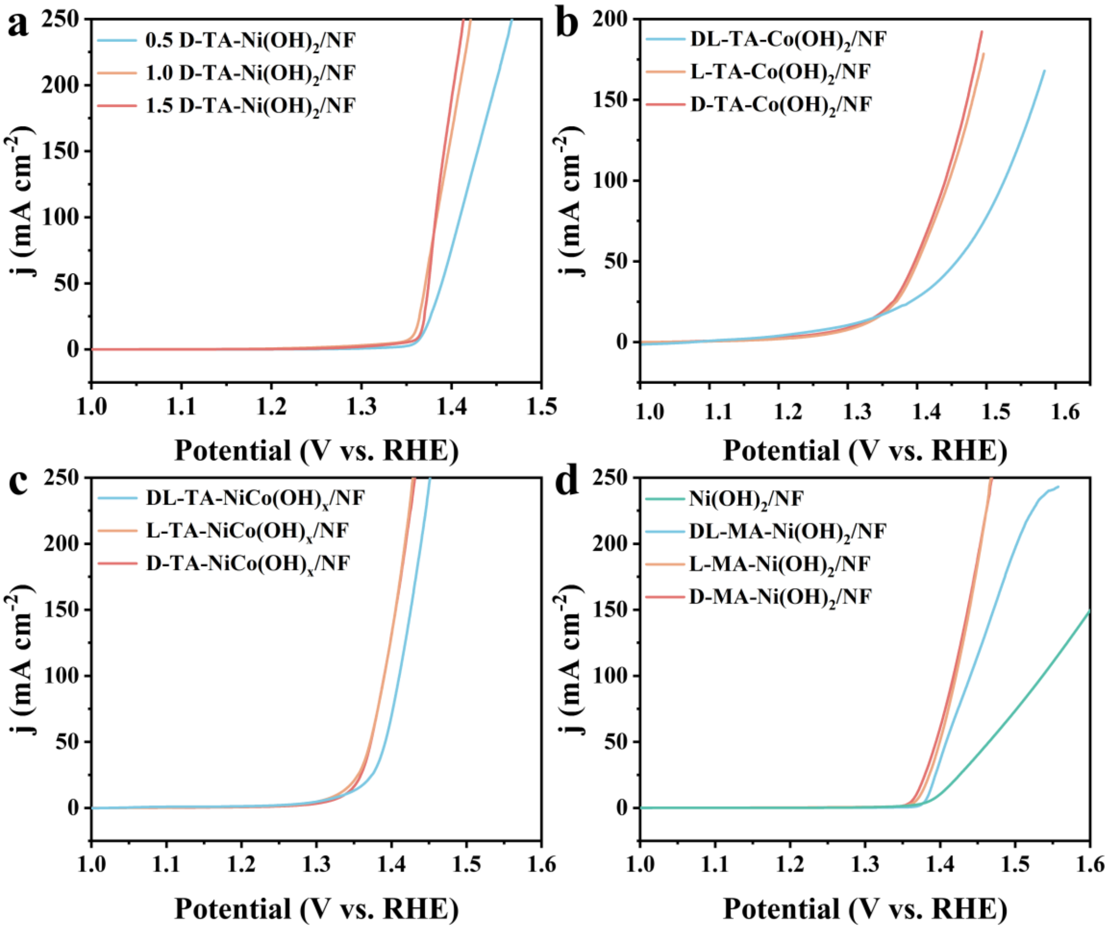

Fig. S15 LSV curves of (a) $Ni(OH)_2$/NF modified with different amount of D-TA; (b) DL-TA-$Co(OH)_2$/NF, L-TA-$Co(OH)_2$/NF and D-TA-$Co(OH)_2$/NF; (c) DL-TA-$NiCo(OH)_X$/NF, L-TA-$NiCo(OH)_X$/NF and D-TA-$NiCo(OH)_X$/NF; (d) $Ni(OH)_2$/NF, DL-MA-$Ni(OH)_2$/NF, L-MA-$Ni(OH)_2$/NF and D-MA-$Ni(OH)_2$/NF.

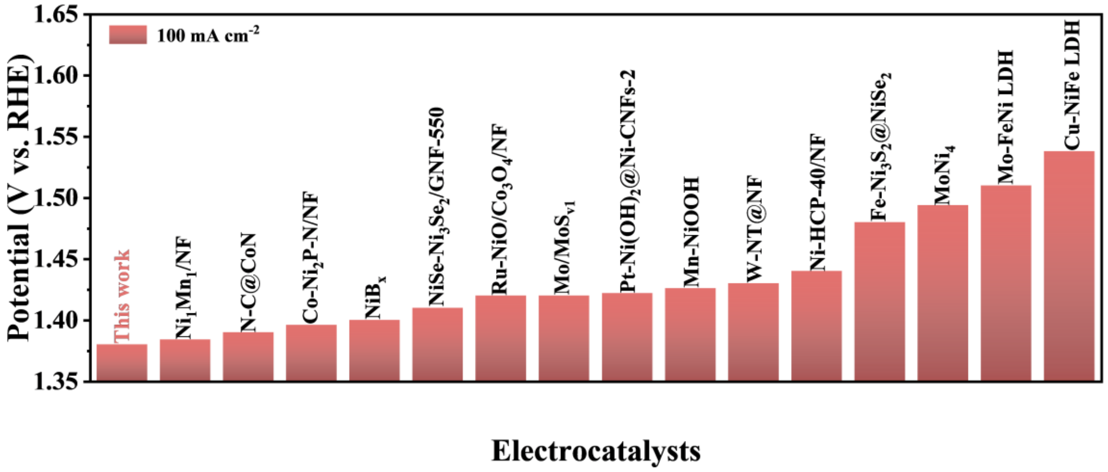

Fig. S16 Comparison of the performance of D-TA-$Ni(OH)_2$/NF with other catalysts at 100 mA cm^{-2}.

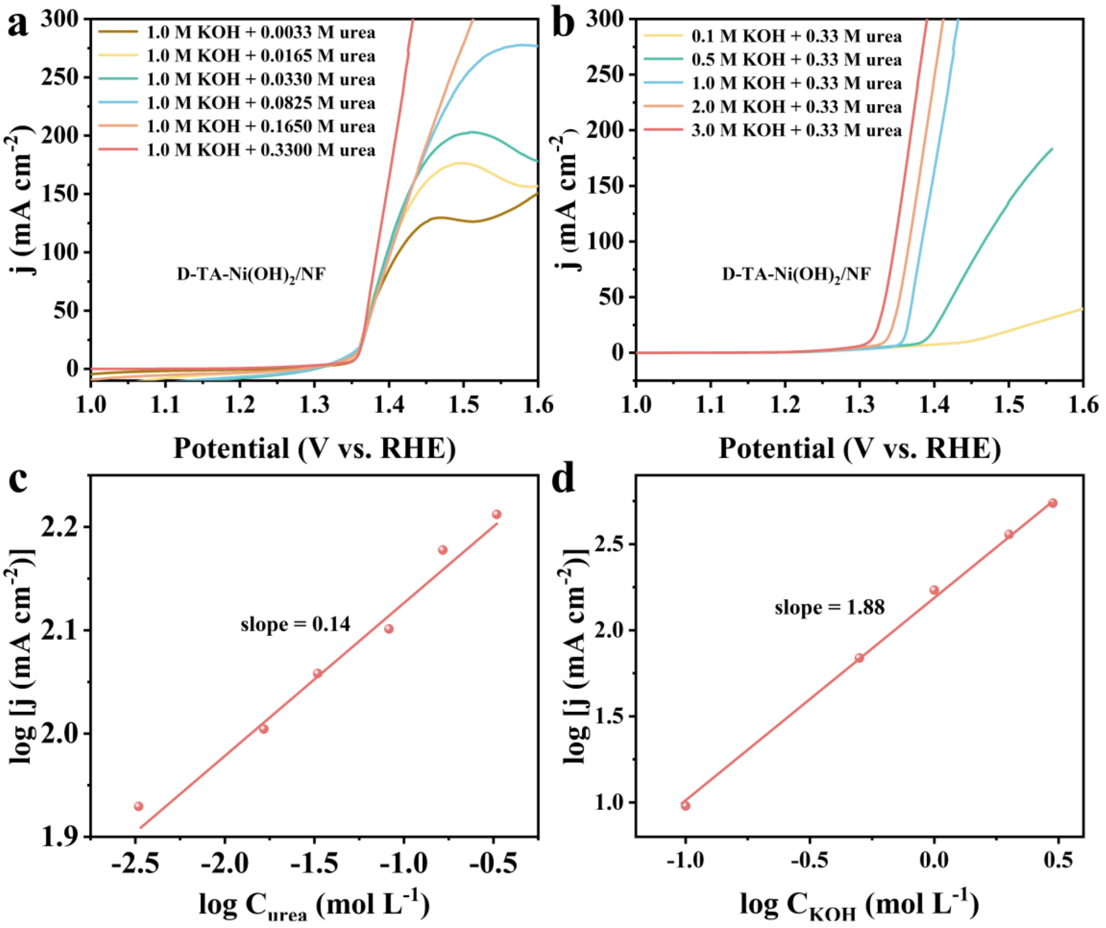

Fig. S17 (a) LSV curves of the D-TA-Ni(OH)$_2$/NF in 1.0 M KOH containing various concentrations of urea. (b) LSV curves of the D-TA-Ni(OH)$_2$/NF in 0.33 M urea containing various concentrations of KOH. (c) The dependence of UOR current density on the urea concentration at 1.40 V. (d) The dependence of UOR current density on the KOH concentration at 1.40 V.

The LSV curves of D-TA-Ni(OH)$_2$/NF in 1.0 M KOH solution with varying urea concentrations were measured, as shown in Fig. S9a. The results indicate that the anodic current density increases with rising urea concentration, suggesting that the UOR is diffusion-controlled at lower urea concentrations.[1] Additionally, the effect of KOH concentration on UOR performance was evaluated in 0.33 M urea solution, as depicted in Fig. S9b. It was observed that the onset potential of the UOR decreased, and the current density significantly increased with increasing KOH concentration, indicating a strong dependence of the UOR process on KOH concentration.

Furthermore, at a constant potential of 1.40 V, the current density was plotted as a function of urea and KOH concentrations in Fig. S9c and Fig. S9d, respectively. The results exhibit linear relationships, with the slopes corresponding to the reaction orders. The reaction order with respect to urea was determined to be 0.14, while that for OH^- was approximately 2, consistent with the reaction pathway reported for most Ni-based electrocatalysts.[2]

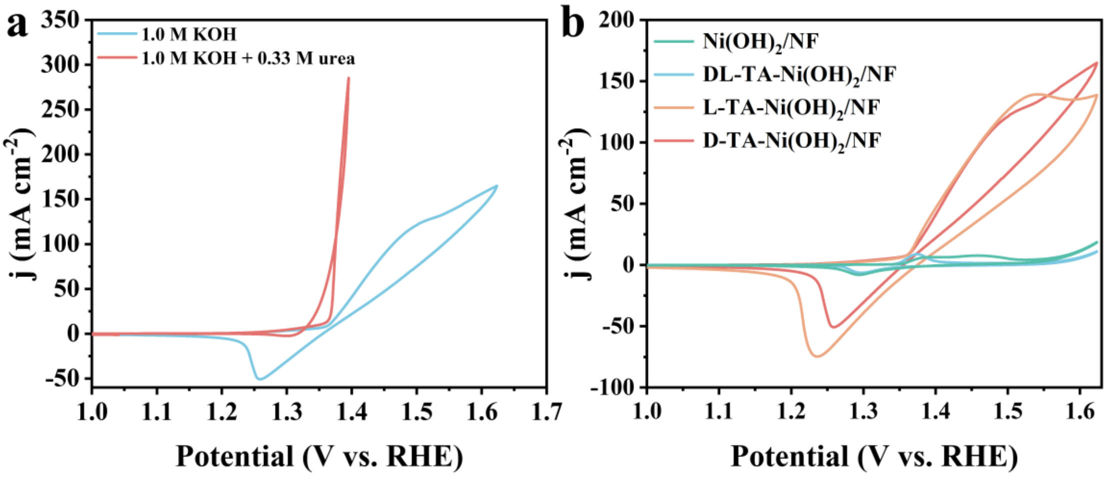

Fig. S18 (a) CV curves of D-TA-$Ni(OH)_2$/NF in 1.0 M KOH with and without 0.33 M urea. (b) CV curves of $Ni(OH)_2$/NF, DL-TA-$Ni(OH)_2$/NF, L-TA-$Ni(OH)_2$/NF and D-TA-$Ni(OH)_2$/NF in 1.0 M KOH.

Table S1. EIS equivalent circuit fitting data of all catalysts.

Catalysts	**R_s (Ω)**	**R_{ct} (Ω)**
$Ni(OH)_2$/NF	1.070	2.735
DL-TA-$Ni(OH)_2$/NF	1.048	0.576
L-TA-$Ni(OH)_2$/NF	1.017	0.466
D-TA-$Ni(OH)_2$/NF	1.012	0.345
DL-MA-$Ni(OH)_2$/NF	1.221	1.667
L-MA-$Ni(OH)_2$/NF	1.139	1.439
D-MA-$Ni(OH)_2$/NF	1.133	1.432
DL-MA-$Co(OH)_2$/NF	1.300	1.609
L-MA-$Co(OH)_2$/NF	1.211	1.500
D-MA-$Co(OH)_2$/NF	1.203	1.488

Table S2. Comparison of different catalysts towards urea oxidation reaction

Sample	**Potential (V vs RHE) at 100 mA cm^{-2}**	**References**
D-TA-Ni(OH)$_2$/NF	1.38	**This work**
Ni$_1$Mn$_1$/NF	1.38	3
N-C@CoN	1.39	4
Co-Ni$_2$P-N/NF	1.40	5
NiB$_x$	1.40	6
NiSe-Ni$_3$Se$_2$/GNF-550	1.41	7
Ru-NiO/Co$_3$O$_4$/NF	1.42	8
Mo/MoS$_{V1}$	1.42	9
Pt–Ni(OH)$_2$@Ni-CNFs-2	1.42	10
Mn-NiOOH	1.43	11
W-NT@NF	1.43	12
Ni-HCP-40/NF	1.44	13
Fe-Ni$_3$S$_2$@NiSe$_2$	1.48	14
MoNi$_4$	1.49	15
Mo-FeNi LDH	1.51	16
Cu-NiFe LDH	1.54	17

References

1. K. Ye, H. Zhang, L. Zhao, X. Huang, K. Cheng, G. Wang and D. Cao, *New J. Chem.*, 2016, **40**, 8673-8680.
2. S.-K. Geng, Y. Zheng, S.-Q. Li, H. Su, X. Zhao, J. Hu, H.-B. Shu, M. Jaroniec, P. Chen and Q.-H. Liu, *Nat. Energy*, 2021, **6**, 904-912.
3. H. Wang, W. Li, L. Meng, Q. Tang, L. Zhang, Y. Ding, C. Li, Y. Sun and H. Wu, *Chem. Eng. J.*, 2024, 158950.
4. T. Tang, C. Li, S. Li, Z. Qiu, T. Yang, B. Ye, S. Shi, C. Wu, F. Cao and X. Xia, *Chin. Chem. Lett.*, 2024, 109887.
5. M. Kim, K. Min, D. Ko, H. Seong, S. E. Shim and S.-H. Baeck, *J. Colloid Interface Sci.*, 2023, **650**, 1851-1861.
6. Y. Hu, L. Shao, Z. Jiang, L. Shi, Q. Li, K. Shu, H. Chen, G. Li, Y. Dong and T. Wang, *Adv. Funct. Mater.*, 2024, 2411011.
7. R. Yin, Z. Wang, J. Zhang, W. Liu, J. He, G. Hu and X. Liu, *Small Methods*, 2401976.
8. J. Li, Y. Lv, X. Wu, R. Xue, Z. Yang, J. Guo and D. Jia, *J. Colloid Interface Sci.*, 2024.
9. F. Gong, Z. Chen, C. Chang, M. Song, Y. Zhao, H. Li, L. Gong, Y. Zhang, J. Zhang and Y. Zhang, *Adv. Mater.*, 2024, 2415269.
10. M. Zhong, M. Xu, S. Ren, W. Li, C. Wang, M. Gao and X. Lu, *Energy Environ. Sci.*, 2024, **17**, 1984-1996.
11. N. Duan, T. Hou, W. Zheng, Y. Qu, P. Wang, J. Yang, Y. Yang, D. Wang, J. Chen and Q. Chen, *ACS Catal.*, 2024, **14**, 1384-1393.
12. M. Liu, W. Zou, S. Qiu, N. Su, J. Cong and L. Hou, *Adv. Funct. Mater.*, 2024, **34**, 2310155.
13. H. Lou, N. Li, R. Zhang, Y. Chen, C. Xie, H. Jiang, Y. Yang and W. Zhang, *Mater. Today Energy*, 2025, **48**, 101779.
14. Y. Zhang, Y. Lei, Y. Yan, W. Cai, J. Huang, Y. Lai and Z. Lin, *Appl. Catal. B Environ. Energy*, 2024, **353**, 124064.
15. X. Wang, N. Sha, N. Zhao, T. Su, C. Lv, L. Yang, Y. Xie and K. Ye, *Chem. Eng. J.*, 2024, **499**, 156119.

16. J. M. Huo, Y. Wang, J. N. Xue, W. Y. Yuan, Q. G. Zhai, M. C. Hu, S. N. Li and Y. Chen, *Small*, 2024, **20**, 2305877.

17. J. Tang, Z. Li, H. Jang, X. Gu, C. Sun, M. G. Kim, L. Hou and X. Liu, *Adv. Energy Mater.*, 2024, **14**, 2403004.